Pang Yuxi (Orcid ID: 0000-0001-5039-0236)

Characterization of anisotropic T2W signals from human knee femoral cartilage: Magic angle effect on spherical surface

Yuxi Pang, PhD

Department of Radiology, University of Michigan, Ann Arbor, MI, USA

Corresponding Author:

Yuxi Pang, PhD
University of Michigan Hospital
1500 E. Medical Center Dr., UH B2 RM A205F
Ann Arbor, MI 48109-5030, USA
Tel: 734-232-6585
Fax: 734-764-2412
Email: yuxipang@umich.edu
Twitter: @yuxipang
ORCID iD: Yuxi Pang (https://orcid.org/0000-0001-5039-0236)

This is the author manuscript accepted for publication and has undergone full peer review but has not been through the copyediting, typesetting, pagination and proofreading process, which may lead to differences between this version and the Version of Record. Please cite this article as doi: 10.1002/nbm.4535

Running Title: Anisotropic T2W signals of femoral cartilage on spherical surface

Word Count: 4,342

ABSTRACT

Purpose: To propose a generalized magic angle effect (gMAE) function for characterizing anisotropic T2W signals of the human knee femoral cartilage with a spherical surface in clinical studies.

Methods: A gMAE model function $f(\alpha, \varepsilon)$ was formulated for an orientation-dependent (ε) transverse T_2 (i.e. $1/R_2$) relaxation in cartilage assuming an axially symmetric distribution (α) of collagen fibers. T2W sagittal images were acquired on an adult volunteer's healthy knee at 3T, and ROI-based average signals $S(\varepsilon)$ were extracted from angularly and radially segmented femoral cartilage. Compared with the standard MAE (sMAE) functions in the deep (DZ, α=0°) and in the superficial (SZ, α=90°) zones, a general form of R_2 orientation-dependent function $f(\alpha, \varepsilon)$ was fitted to $S(\varepsilon)$, including an isotropic R_2 contribution (REF). Goodness of fit was evaluated by root-mean-square deviations (RMSD). An F-test and a paired t-test were respectively used to assess significant differences between the observed variances and means, with statistical significance set to $P < .05$.

Results: As a symmetric orientation-dependence function with a varying dynamic range, the proposed gMAE model outperformed the pervious sMAE functions manifested by significantly reduced RMSDs in the DZ (0.239±0.122 vs. 0.267±0.097, P=.014) and in the SZ (0.183±0.081 vs.

0.254±0.085, P<.001). The fitted average angle α (38.5±34.6° vs. 45.1±30.1°, P<.43) and REF (5.092±0.369 vs. 5.305±0.440, P<.001) were smaller in the DZ than those in SZ, in good agreement with the reported collagen fibril microstructural configurations and the non-bound water contribution to R_2 in articular cartilage.

Conclusion: A general form of the magic angle effect function was proposed and demonstrated for better characterizing anisotropic T2W signals from the human knee femoral cartilage at 3T in clinical studies.

Keywords: magic angle effect, spherical surface, human knee femoral cartilage, residual dipolar interaction, orientation-dependent transverse relaxation, anisotropic T2 weighted imaging.

Abbreviations: ARCADE, anisotropic R_2 of collagen degeneration; DZ, deep zone; FOV, field of view; MAE, magic angle effect; HR, high-resolution; LFC, lateral femoral condyle; MFC, medial femoral condyle; REF, internal reference; RDC, residual dipolar coupling; RMSD, root-mean-square deviation; ROI, region of interest; SENSE, sensitivity encoding; SZ, superficial zone; T2W, T2-weighted image; TE, echo time; TZ, transitional zone.

1 | INTRODUCTION

Magic angle effect (MAE) is a well-known phenomenon of anisotropic transverse T_2 (i.e. $1/R_2$) relaxation in MR imaging of highly ordered biological tissues such as tendons and articular

cartilage,[1-3] yet its potential in unraveling physiological and pathological changes has not been fully exploited.[4,5] For tendons and cartilage, MAE originates from some restricted water molecules buried inside collagen triple-helical microstructures,[6,7] manifested by residual dipolar coupling (RDC) between two water protons that is proportional to a spatial factor $\langle 3\cos^2\theta - 1\rangle$.[8-10] Herein, an internuclear dipolar interaction vector makes an angle θ relative to the static magnetic field B_0, and an ensemble or time average is represented by angle brackets. It should be mentioned that MAE does not exclusively belong to collagen – a major cable-like structural protein in the human body.[11] Regardless of distinct water residing environments, MAE will appear whenever water molecular reorientations are somewhat hindered.[12-14] In an isotropic liquid solution, RDC will vanish due to unrestricted and rapid water molecular motions; on the other hand, the specific spatial factor $\langle 3\cos^2\theta - 1\rangle$ could also become zero in an anisotropic environment given that the relevant water molecules are orientated preferentially with θ=54.7°, the so-called magic angle (MA).[3,8]

When the MA condition is fulfilled, an anisotropic transverse relaxation $R_2^a(\theta)$ in highly ordered biological tissues will disappear resulting in the widely reported hyper-intensity T_2-weighted images in the literature.[1,3] It is worthwhile to emphasize that $R_2^a(\theta)$ is determined by the variance of RDC, i.e. $\langle(3\cos^2\theta - 1)^2\rangle$, rather than RDC itself.[9,10] For knee articular cartilage, R_2 could be conveniently categorized into an isotropic R_2^i and an anisotropic $R_2^a(\theta)$ components,[9,10,15] with the latter specifically associated with the integrity of collagen fibril ultrastructures.[4,5,16] With respect to other relaxation metrics that have been studied to date, R_2 is reportedly the most susceptible to orientation anisotropy, but with the best sensitivity in detecting

cartilage early degenerations due to osteoarthritis.[4] If the isotropic component had been removed from R_2, the resulting R_2, i.e. $R_2^a(\theta)$, would have possessed markedly improved specificity in revealing biochemical and microstructural changes well before visible morphologic alterations.[17-19] Unfortunately, R_2^i and $R_2^a(\theta)$ are not commonly separated from each other in the conventional R_2 mapping in clinical studies of the human knee articular cartilage.

Recently, an efficient $R_2^a(\theta)$ mapping method, referred to as ARCADE,[20] has been proposed based on a single T2W sagittal image in which an internal reference (REF) is exploited for separating $R_2^a(\theta)$ from its counterpart R_2^i in the human knee femoral cartilage at 3T. This particular REF must be deduced from the MA orientation of collagen fibers in the deep zone (DZ), by fitting the standard magic angle effect (sMAE) function, i.e. $\langle(3\cos^2\theta - 1)^2\rangle$, to angularly segmented T2W signals. It was surprisingly found that the commonly used sMAE function was only adequate for characterizing a few sagittal imaging slices.[20] The reliability of the determined REF could have been markedly improved if it had been derived from more imaging slices than otherwise.

As illustrated in Figure 1A, the human knee femoral cartilage has a curved surface because of two extruding condyles, i.e. lateral (LFC) and medial (MFC) femoral condyles,[21,22] which could be approximately described by a spherical surface. Even though a circle could be defined for the angularly segmented femoral cartilage in a sagittal imaging plane,[20,21,23] the normal vector ($\vec{m}$) to cartilage surface imaged in a lateral or medial slice (green box) will deviate from those ($\vec{n}$) imaged close to the central condyles (red box) as depicted schematically in a coronal plane (Figure 1B)

and a unit sphere (Figure 1C). These unusual locations of off-center imaging slices are not compatible with what has been typically assumed in the sMAE function in which the cartilage surface normal could be parallel along B_0 and within the imaged sagittal slice. Without taking into account the fact that the femoral cartilage has an irregular surface, some previously reported clinical R_2 anisotropy measurements would have appeared to be contradictory with the well-established MAE.[23,24]

On the other hand, the collagen fibril microstructural distributions from the uppermost (i.e. cartilage surface) to the innermost layers of articular cartilage are extremely complex.[25,26] In the past, various models have been developed for characterizing the detailed fibril architectures in both the animal and the human tissues. In a microscopy MR imaging (μMRI) 7T study of canine humeral heads at an extremely high resolution,[26] three models (i.e. solid cone, funnel and fan) of fibril configurations have been extensively investigated and the collagen fibril distributions in the superficial zone (SZ) was reportedly better characterized by a combination of the first two models while the third model was the choice for those in the DZ. In another prior T2W study on healthy human knees at 7T,[27] the solid cone model was also used for quantifying the depth-dependent anisotropic cartilage architecture. Unlike the previously reported *ex vivo* study,[26] an analytical function for the solid cone model was provided; but, this specific function became valid only within a limited orientation range for fibril distributions from DZ to the transitional (TZ) zone. In other words, this particular model was not suitable for quantifying collagen microstructures in the SZ of the human knee articular cartilage.

In clinical 3T studies of orientation-dependent T2W imaging of the human knee femoral cartilage, two halves of cartilage layers, i.e. DZ and SZ, are usually partitioned due to a limited imaging resolution as shown schematically in Figure 2B.[20,23] It should be pointed out that the segmented DZ most likely includes multiple layers with fibril microstructures orientated differently from $\vec{n}$, and the segmented SZ covers at least both the histologically defined the SZ and TZ of the femoral cartilage[28,29] as illustrated in Figure 2A, where the collagen fibril histological distributions diverge continuously from DZ to SZ based on the well-known arcade model,[30,31] and are further depicted by the funnel model using different α angles.[26]

While T2W anisotropies in an ideal DZ or SZ layer could be respectively characterized by the sMAR function of $(3\cos^2\theta - 1)^2$ or $(1 - 3\sin^2\theta + (27/8)\sin^4\theta)$;[9,30] a general form of the magic angle effect (gMAE) function must be sought to quantify realistic fibril microstructural configurations in angularly segmented femoral DZ and SZ cartilage on a curved surface. In order to better characterize anisotropic T2W images of the human knee articular cartilage from clinical studies and derive a less biased REF and thus a reliable anisotropic R_2 relaxation metric independent of T2W pulse sequences,[20] the curved nature and multiple-layer aspect in the femoral cartilage ought to be considered in the conventional MAE model. Therefore, this work aimed to propose a theoretical gMAE framework to meet an unmet need and demonstrate its performance on an asymptomatic knee of one adult volunteer at 3T, with respect to the commonly used sMAE models.

2 | METHODS

2.1 | Theory

Water proton intramolecular dipolar interactions in collagen-rich tissues are, on average, along the fiber bundles' primary direction.[6,7,9] With respect to the surface normal ($\vec{n}$) in cartilage, the collagen fibril microstructures are, as depicted in Figure 2A, predominantly orientated perpendicularly, at random and in parallel in the SZ, TZ, and DZ, respectively.[29,30] Given an image voxel comprising the fibril microstructures distributed in an axially symmetric system when $\vec{n}$ is not aligned with B_0 as shown in Figure 3A,[9,26] the orientation dependence of an anisotropic transverse relaxation $R_2^a(\theta)$ of water protons in cartilage can be derived from an ensemble average of dipolar interactions associated with differently orientated fibers, i.e. $\langle(3\cos^2\theta - 1)^2\rangle$.

In this oversimplified symmetric model, an exact distribution of collagen fibers could be adequately characterized by two constant angles α and ε, along with two varying angles θ and φ. Specifically, a representative fiber forms an angle α with $\vec{n}$ that in turn makes an angle ε with B_0. An angle θ is formed between the fiber and B_0, and an angle φ is an azimuthal angle of the fiber ranging from 0 to 2π. In order to evaluate an orientation (i.e. θ) dependence function in terms of angles α and ε, i.e. $f(\alpha,\varepsilon)=\langle(3\cos^2\theta - 1)^2\rangle$, the term $\cos\theta$ has to be recast using other trigonometric forms containing α, ε and φ, and an ensemble average has to be taken over all φ angles.

According to the spherical law of cosines, the term $\cos\theta$ can be expressed by $(\cos\alpha\cos\varepsilon + \sin\alpha\sin\varepsilon\cos\varphi)$. As a result, the subfunction of $(3\cos^2\theta - 1)$ could be

represented by a three-termed expression, i.e. $(1/2)(3\cos^2\alpha - 1)(3\cos^2\varepsilon - 1) + (3/2)\sin^2\alpha\sin^2\varepsilon\cos 2\varphi + (3/2)\sin 2\alpha \sin 2\varepsilon \cos\varphi$.[32] After this subfunction having been squared and then taken an ensemble average, $f(\alpha, \varepsilon)$ could be simply expressed by Equation 1. It should be noted that all trigonometric terms containing either $\langle\cos\varphi\rangle$ or $\langle\cos 2\varphi\rangle$ become zero.

$$f(\alpha,\varepsilon) = (1/4)\{(3\cos^2\alpha - 1)^2(3\cos^2\varepsilon - 1)^2\} + (9/8)\{(\sin\alpha\sin\epsilon)^4 + (\sin 2\alpha \sin 2\epsilon)^2\}. \quad (1)$$

Even though it appears markedly different from what has been presented in his seminal paper by Berendsen,[9] $f(\alpha, \varepsilon)$ will give the same orientation dependence except for a scaling factor 9/4. This axially systematic model was referred to as the funnel model in the literature but without an analytical function.[26] When α=0° and 90°, $f(\alpha, \varepsilon)$ will restore the sMAE functions previously used in the DZ and SZ, respectively.[30]

One salient feature of $f(\alpha, \varepsilon)$ is its multitude symmetries originated from the characteristics of an axially symmetric model as revealed in both Eq. 1 and Figure 3C. Accordingly, the observed orientation dependence could be interpreted as α variations while keeping ε constant, and vice versa. As shown in Figure 1A, the femoral cartilage has a curved surface, and it is infrequent for the surface normal to be parallel to B_0 in standard sagittal images. From angularly segmented ROIs, an orientation dependent form can be always derived regardless of its association with the surface normal as schematically demonstrated for one imaging slice (green) in Figure 1C.

When an imaging slice deviates from the center of the femoral condyles, its surface normal $\vec{m}$ will make an angle α with $\vec{n}$ from the central slice when ε=0, assuming that the femoral condyle

has an ideally half-sphere shape. Mathematically, it is indistinguishable between $f(\alpha, \varepsilon)$ and $f(\varepsilon, \alpha)$; as a result, it is appropriate to quantify the orientation dependences (ε) for all imaging slices with an adjustable parameter α to account for the differences not only in sagittal slice locations but also in fibril architectures across the femoral cartilage layers.

2.2 | T2W MR imaging of human knee cartilage

T2W sagittal images were acquired using an interleaved multi-slice (n=32) multi-echo (n=8) turbo spin echo sequence, with a 16-channel T/R knee coil on an Ingenia 3T MR scanner (Philips Healthcare, Best, The Netherlands). Some key acquisition parameters were listed as follows: field of view = 128*128*96 mm^3; acquired/reconstructed voxel size = 0.6*0.6*3.0 / 0.24*0.24*3.0 mm^3; Compressed SENSE [33] factor = 2.5; image readout bandwidth = 443.3 Hz; TR = 2500 ms; TEs = n*6.1 ms with n=1-8; and total scan time = 7.42 minutes. In this study, only T2W images with TE of 48.8 ms were evaluated from an asymptomatic right knee of one consented male (35 yrs) subject in an IRB-approved clinical study.

A high-resolution (HR) 3D image of the same knee was also acquired using the turbo spin echo sequence with a variable flip angle excitation scheme. FOV was 129*129*129 mm^3 and acquired voxel size was 0.52*0.52*0.52 mm^3, which was then interpolated to 0.26*0.26*0.26 mm^3. An effective TE and TR were 37 and 1000 ms, respectively. With a Compressed SENSE reduction factor of 3, the total scan time was 5.1 minutes. This HR dataset was used only for visualization purposes in the current study.

2.3 | Angular and radial segmentations

The femoral cartilage was first manually delineated on each of T2W sagittal imaging slices using a free software ITK-SNAP.[34] Next, a large circle was fitted to the whole femoral cartilage from which angularly segmented ROIs were partitioned with an angular resolution of 5°, each with an estimated angle β relative to B_0, which pointed downward in the image (see Figure 4). These estimated β angles, which were assumed to be aligned with the varying normal vectors on the curved cartilage surface, were further refined based on locally defined circles using only adjacent ($\beta \pm 10°$) spatial information to better represent the normal vector ($\vec{n}$) in the femoral cartilage.[20] Finally, these angularly segmented ROIs were further subdivided into the DZ and SZ equally in the radial direction.

2.4 | Modeling anisotropic T2W signals

An average T2W signal intensity, S, from one segmented ROI in femoral cartilage could be conveniently expressed by Equation 2 as follows,

$$S = S_0 \exp\left\{-\left(R_2^i + R_2^a * f(\alpha, \varepsilon)\right) TE\right\} \qquad (2)$$

$$y(\varepsilon) = A - B * f(C, \varepsilon) \qquad (3)$$

where S_0, R_2^i, $R_2^a * f(\alpha, \varepsilon)$ and TE represented an initial signal intensity when TE=0, an isotropic and an anisotropic R_2, and an echo time, respectively. In a logarithmic scale, Eq. 2 was transformed into Eq. 3, which was the anisotropic R_2 model used to fit the segmented orientation-dependent data from any imaging slices.

For this particular anisotropic R_2 model, ε was an independent variable and the three fitted model parameters were as follows: $A = \left(Log\, S_0 - R_2^i TE\right)$, also called an REF in the

literature;[20] B=R_2^a*TE; and C= α. Once a global REF was determined, an anisotropic R_2 could be simply calculated as $(A - \log S)/TE$ as demonstrated before using a single T2W image.[20] Clearly, when an REF was underestimated, so would be the derived anisotropic R_2, thereby increasing the possibility of becoming non-physical negative relaxation values. For comparative purposes, the three-parameter data fitting using Eq. 3 was labeled as "gMAE" for both the DZ and SZ data, whereas the two-parameter fitting for both the DZ (C= 0°) and SZ (C=90°) data were referred to as "sMAE".

2.5 | Nonlinear least-squares fitting

Data modeling was performed by minimizing the total χ^2 value, defined as the sum of squared deviates between the model and the measured data. These residuals had been normalized by the corresponding measurement uncertainties (i.e. 1-σ standard deviations). The χ^2 minimization was accomplished using a publicly available IDL script (http://purl.com/net/mpfit) based on the Levenberg-Marquardt technique for nonlinear least-squares curve fitting.[35] During the χ^2 optimization processes, the fitting parameters were constrained as follows: A=[3, 7]; B=[0.01, 2] and C=[0, 90°], with the first two determined heuristically. The maximum number of iterations was limited to 200 for one set of initial values of fitting parameters within their constraints, and five sets of different starting values were used to prevent from being trapped in the local minima.[36]

The root-mean-square deviation (RMSD) was calculated as a measure of goodness of fit. An F-test was performed to assess the statistical significance of the goodness of fit, based on the RMSD calculated from two models. A P-value was then derived from F-distribution, with

significance indicated by $P < .05$. Additionally, a paired *t*-test was used with significance set to $P < .05$, assessing the mean differences between two fitted parameters. All image and data analysis were completed with customized software developed in IDL 8.5 (Harris Geospatial Solutions, Inc., Broomfield, CO, USA). Unless indicated otherwise, all the fitted data were represented as mean ± standard deviation.

3 | RESULTS

3.1 | Theoretical anisotropic R_2 orientation dependence $f(\alpha, \varepsilon)$

Figures 3B-D present $f(\alpha, \varepsilon)$ as four characteristic profiles (B) with α=0° (red), 33° (green), 57° (blue) and 90° (black), a 2D distribution map (C), and a 3D multiple (n=11) layers quarter-sphere (D) with α ranging from 0° (innermost) to 90° (outermost). An ideal imaging slice (i.e. XZ plane at Y=0, with only two layers) is depicted in Figure 2C, showing the expected femoral cartilage R_2 orientation-dependence $f(0°, \varepsilon)$ and $f(90°, \varepsilon)$ in the DZ and SZ, respectively.

Some prominent features of $f(\alpha, \varepsilon)$ are deserved mentioning. First, the dynamic range of $f(\alpha, \varepsilon)$ is markedly different depending on α. For instance, $f(0°, \varepsilon)$ has the largest range spanning from 0 (ε=54.7°) to 4 (ε=0°); on the other hand, it becomes hardly orientation-dependent when ε changed from 0° to 50° with α=33° (see Fig. 3B). Second, the magic angle for $f(\alpha, \varepsilon)$ will magically disappear when $\alpha \neq 0°$, i.e. $f(\alpha, \varepsilon) \neq 0$. Third, the multitude symmetries of $f(\alpha, \varepsilon)$ manifest that $f(\alpha, \varepsilon) = f(\alpha, \varepsilon \pm 180°)$, $f(\alpha, 90° - \varepsilon) = f(\alpha, 90° + \varepsilon)$, and $f(\alpha, \varepsilon) = f(\varepsilon, \alpha)$ as demonstrated in Figure 3C.

3.2 | Modeling T2W signals of femoral cartilage

A regional volume-rendered HR right knee is shown in Figure 1A, highlighting the curved nature of cartilage surfaces from medial (MFC) and lateral (LFC) femoral condyles. Figure 4B pinpoints the spatial locations on an HR coronal image of six representative T2W sagittal images from the MFC (S05, S09, and S13) and the LFC (S20, S25, and S29). Two sagittal imaging slices approximately cutting through the central condyles are presented in Figures 4A (S25) and 4C (S09), with the angularly and radially segmented ROIs superimposed.

Figure 5 depicts the exemplary MFC image slices (1st column), i.e. Slices 05 (5A), 09 (5B, Fig. 4C) and 13 (5C), with the measured (black circles) and fitted (gMAE, solid red lines; sMAE, dashed green lines) segmented T2W signals in the DZ (2nd column) and SZ (3rd column). Similarly, Figure 6 demonstrates the three LFC image slices, i.e. Slices 20 (6A), 25 (6B, Fig. 4A) and 29 (6C), and fitting results. Table 1 tabulates the resulting fitted parameters of these six representative imaging slices.

In general, gMAE provided significantly ($P<.01$) better fits for the edged imaging slices when compared with sMAE, for instance, for Slice 05 and Slice 29 in the DZ, and Slice 20 in the SZ. Compared to those changes between in the DZ and in the SZ from the central imaging slices, the observed T2W signal fluctuations from the edged slices appeared more similar to (e.g. Slice 20) or even reversed (e.g. Slice 29) from each other, signifying a curved nature of the femoral cartilage when deviated from the central condyles. These observations were in good agreement with the theoretical predictions as shown in Figure 3.

As demonstrated by the RMSDs of the fits for all imaging slices in Figure 7A, gMAE on average significantly outperformed sMAE in the DZ (0.239±0.122 vs. 0.267±0.097, P=.014) and in the SZ (0.183±0.081 vs. 0.254±0.085, P<.001). Comparing gMAE with sMAE as shown in Figure 7B, the fitted parameter A (i.e. REF) was significantly larger in the DZ (5.092±0.369 vs. 4.850±0.177, P<.001) and in the SZ (5.305±0.440 vs. 5.035±0.155, P<.001). In addition, a relatively smaller average angle α was observed in the DZ when compared to that in the SZ, i.e. 38.5±34.6° vs. 45.1±30.1°, P<.43, largely consistent with the reported fibril microstructural arrangements from the DZ to the SZ in articular cartilage.[3,27]

When taking an average fitted A from both DZ and SZ as a global REF, the derived anisotropic R_2 maps of the femoral cartilage are presented in Figures 7C and 7D using gMAE fitting and in Figures 7E ad 7F using sMAE fitting, in both the DZ (7C and 7E) and SZ (7D and 7F). A relatively larger REF (i.e. 5.20 vs. 4.94) when compared gMAE with sMAE fitting resulted in a markedly reduced number of non-physical negative anisotropic R_2 values, suggesting that the proposed gMAE model could considerably improve the characterization of anisotropic R_2 of the human knee femoral cartilage on a curved surface.

4 | DISCUSSION

In this work, a generalized orientation dependence $f(\alpha, \varepsilon)$ function for anisotropic R_2 relaxation has been proposed for better characterizing the MAE in the human knee femoral cartilage that features an irregular surface. This proposed gMAE model was first evaluated by simulations and

then demonstrated on an adult volunteer's asymptomatic knee. Compared with the conventional sMAE functions, the proposed gMAE model has provided a significantly improved explanatory power to account for anisotropic T2W signals both in the DZ and in the SZ, and thus a less biased REF could be derived from which a more reliable anisotropic R_2 relaxation metric could be determined from a single T2W image.

The theoretical framework presented in this work is not particularly different from what has been shown in 1962 by Berendsen in his seminal paper.[9] However, an orientation dependence functional form $f(\alpha, \varepsilon)$ given by Eq. 1 sheds more light on the underlying axially symmetric model when compared with his original expanded function that merely provides the same results. Not only does the proposed $f(\alpha, \varepsilon)$ clearly show the multitude symmetries, but it also predicts that the magic angle (i.e. 54.7°) magically disappears when $\alpha \neq 0°$; in other words, $f(\alpha, \varepsilon)$ can be zero only when $\alpha = 0°$. This interesting finding could be significant when considering of an REF derived from the MA orientations.[20] The data listed in Table 1 shows that only three out of six fitted α in the DZ were zero; in fact, considering all segmented sagittal slices (n=26), there would be more than 70% of the nonzero fitted α angles in the DZ (data not shown).

For clinical T2W imaging of the human knee articular cartilage at 3T, an attainable imaging resolution is far more less than what could be measured *ex vivo* using μMRI; for instance, the acquired in-plane resolution in this work was 600 x 600 μm^2 with the slice thickness of 3 mm, in contrast to 26 x 13 μm^2 with the slice thickness of 1 mm as previously reported.[26] Although intrinsically complex, the depth-dependent collagen fibril microstructures studied by clinical T2W

imaging at 3T might be adequately described using a simple analytical function $f(\alpha, \varepsilon)$ that has been proposed herein. It is worthwhile to point out that $f(\alpha, \varepsilon)$ is just an analytical function for the previously mentioned funnel model.[26]

Referred to an REF in the literature,[20] the fitted model parameter A typically encoded information about non-bound water proton density and isotropic T_2 and T_1 (but not anisotropic T_2) relaxation effects. This particular model parameter is directly linked to an anisotropic R_2, i.e. $R_2^a f(\alpha, \varepsilon) = (A - logS)/TE$, derived from a single T2W image using the previously developed ARCADE method;[20] thereby, an underestimated A would be translated into a reduced anisotropic R_2 that could become a negative value. When $\alpha \neq 0$ as the most cases in the femoral cartilage, the highest segmented T2W signals in the DZ, originally thought to be from the MA locations, would most likely contain the contributions from an anisotropic R_2 because of nonzero $f(\alpha, \varepsilon)$. As a result, the REF derived from the conventional approach was noticeably reduced (see Figure 7B), resulting in an relatively increased number of negative anisotropic R_2 as shown in Figures 7E and 7F. It should be noted that the REF from the gMAE model was slightly smaller in the DZ than that in the SZ, i.e. 5.092±0.369 vs. 5.305±0.440. Although this REF difference was small (i.e. about 6%), it was indeed significant (P=.014), in good agreement with previous findings.[37-39]

As predicted by the gMAE model (see Figure 3B), the dynamic range of $f(\alpha, \varepsilon)$ depends significantly on a particular fibril microstructural configuration (i.e. α). For example, Slice 29 (see Figures 4B and 6C) cut through an edge of the lateral femoral condyle, presenting a greater MAE variation in the SZ than that in the DZ. This interesting observation could not be explained by the

sMAE model that has been commonly used in the preclinical studies on T_2 orientation anisotropy. In those experimental studies, the cartilage surface normal vector direction ($\vec{n}$) was always carefully positioned so that the MAE could become maximized, i.e. $\vec{n} \parallel B_0$.

Surprisingly, Mosher et al. also reported previously a similar result as what was observed for Slice 29 in this work, calling into question the validity of the (standard) MAE in the femoral cartilage.[24] It was not surprising that his unexpected finding had led to a heated debate among the researchers,[40-42] and one of them had correctly *predicted* that the curved cartilage surface was responsible for the seemingly contradictory result.[42] The present study actually provides a needed theoretical framework for adequately understanding the complex nature of anisotropic R_2 of the human knee femoral cartilage. With this developed model, it is not difficult to comprehend the previous findings that some R_2 or $R_{1\rho}$ values in the femoral SZ cartilage became even higher than those found in the corresponding DZ.[23,43]

In biological tissues, highly structured macromolecules and their assemblies are ubiquitous; thereby, water proton anisotropic R_2 relaxation becomes a commonplace phenomenon in MR imaging of these highly ordered tissues.[1,44] When interpreting the orientation-dependent transverse relaxation effect originated from a specific highly organized tissue such as the human brain white matter, neither should MAE be linked exclusively to the content of collagen, nor should the residual dipolar interactions be considered orientating in the same direction (i.e. $\alpha = 0$).[45] The proposed gMAE model could possibly find a wide variety of applications in quantifying

orientation-dependent R_2 relaxation in highly ordered tissues beyond the human knee articular cartilage.

It should be mentioned that some limitations exist in this study. First, the orientation information about an angle ε was heavily dependent on the manual segmentation's accuracy of the femoral cartilage. One of the confounding factors would be a poorly defined cartilage-bone interface. In principle, the developed advanced MR imaging methods such as diffusion and susceptibility tensor imaging techniques[46,47] could provide more accurate collagen fibrils orientation information albeit at the cost of scanning times and the efforts involved in image post-processing. Second, the human knee articular cartilage network microstructures are age-dependent,[30] while the femoral cartilage studied in this work was from an adult subject's knee. It thus remains unclear whether or not the proposed gMAE model will be applicable to younger subjects with underdeveloped cartilage microarchitectures. Third, the articular cartilage three-dimensional microstructures are extremely complex varying across different layers, particularly on the SZ where two distinct anisotropic components have been previously reported.[26] Hence, it should not be surprising that the proposed gMAE model sometimes does not fit well the segmented femoral cartilage. Finally, although the isotropic chemical exchange effect has not been considered in this work, it still contributed a few percent to R_2 in cartilage at 3T.[20,48] Towards the MA locations, this specific contribution would be increasingly important because the dominant dipolar interactions became increasingly close to zero. Therefore, the determined REF was slightly underestimated at 3T, and this confounding effect would be exacerbated at higher B_0 fields.

5 | CONCLUSIONS

A general form of the magic angle effect function has been proposed and demonstrated for better characterizing anisotropic T2W signals from the human knee femoral cartilage. As a result, a more reliable internal reference could be determined leading to more accurate collagen-specific anisotropic R_2 relaxation rates derived efficiently from a single T2W image. The potential applications of the proposed generalized MAE model could be extended to other highly organized biological tissues even though the current work focused on cartilage.

ACKNOWLEDGEMENTS

We would like to thank Suzan Lowe and James O'Connor for help in collecting the human knee cartilage images. This work was in part supported by the Eunice Kennedy Shriver National Institute of Child Health & Human Development of the National Institutes of Health (NIH) under Award Number 5-R01-HD-093626-02 (to Prof. Riann Palmieri-Smith). The content is solely the responsibility of the author and does not necessarily represent the official views of the NIH.

DATA AVAILABILITY STATEMENT

Data available on request from the author.

REFERENCES

1. Bydder M, Rahal A, Fullerton GD, Bydder GM. The magic angle effect: a source of artifact, determinant of image contrast, and technique for imaging. *J Magn Reson Imaging.* 2007;25(2):290-300.
2. Fullerton GD. The magic angle effect in NMR and MRI of cartilage. In: Xia Y, Momot KI, eds. *Biophysics and Biochemistry of Cartilage by NMR and MRI*. Cambridge, UK: The Royal Society of Chemistry; 2016:109-144.
3. Xia Y. Magic-angle effect in magnetic resonance imaging of articular cartilage: a review. *Invest Radiol.* 2000;35(10):602-621.
4. Hanninen N, Rautiainen J, Rieppo L, Saarakkala S, Nissi MJ. Orientation anisotropy of quantitative MRI relaxation parameters in ordered tissue. *Sci Rep.* 2017;7(1):9606.
5. Pang Y. An order parameter without magic angle effect (OPTIMA) derived from R1ρ dispersion in ordered tissue. *Magn Reson Med.* 2020;83(5):1783-1795.
6. Fullerton GD, Rahal A. Collagen structure: The molecular source of the tendon magic angle effect. *Journal of Magnetic Resonance Imaging.* 2007;25(2):345-361.
7. Tourell MC, Momot KI. Molecular dynamics of a hydrated collagen peptide: insights into rotational motion and residence times of single-water bridges in collagen. *J Phys Chem B.* 2016;120(49):12432-12443.
8. Erickson SJ, Prost RW, Timins ME. The Magic-Angle Effect - Background Physics and Clinical Relevance. *Radiology.* 1993;188(1):23-25.
9. Berendsen HJC. Nuclear magnetic resonance study of collagen hydration. *J Chem Phys.* 1962;36(12):3297-3305.
10. Momot KI, Pope JM, Wellard RM. Anisotropy of spin relaxation of water protons in cartilage and tendon. *NMR Biomed.* 2010;23(3):313-324.
11. Bella J. Collagen structure: new tricks from a very old dog. *Biochem J.* 2016;473:1001-1025.
12. Woessner DE. Nuclear magnetic-relaxation and structure in aqueous heterogenous systems. *Mol Phys.* 1977;34(4):899-920.
13. Totland C, Nerdal W. Experimental Determination of Water Molecular Orientation near a Silica Surface Using NMR Spectroscopy. *The Journal of Physical Chemistry C.* 2016;120(9):5052-5058.
14. Fung B. Orientation of water in striated frog muscle. *Science.* 1975;190(4216):800-802.
15. Peto S, Gillis P, Henri VP. Structure and dynamics of water in tendon from NMR relaxation measurements. *Biophysical journal.* 1990;57(1):71-84.
16. Lenk R, Bonzon M, Greppin H. Dynamically oriented biological water as studied by NMR. *Chemical Physics Letters.* 1980;76(1):175-177.
17. Link TM, Neumann J, Li X. Prestructural Cartilage Assessment Using MRI. *J Magn Reson Imaging.* 2017;45(4):949-965.
18. Roemer FW, Kijowski R, Guermazi A. Editorial: from theory to practice - the challenges of compositional MRI in osteoarthritis research. *Osteoarthritis Cartilage.* 2017;25(12):1923-1925.

19. Link TM, Li X. Establishing compositional MRI of cartilage as a biomarker for clinical practice. *Osteoarthritis and Cartilage.* 2018;26(9):1137-1139.
20. Pang Y, Palmieri-Smith RM, Malyarenko DI, Swanson SD, Chenevert TL. A unique anisotropic R2 of collagen degeneration (ARCADE) mapping as an efficient alternative to composite relaxation metric (R2 -R1 rho) in human knee cartilage study. *Magn Reson Med.* 2019;81(6):3763-3774.
21. Monk AP, Choji K, O'Connor JJ, Goodfellow JW, Murray DW. The shape of the distal femur: a geometrical study using MRI. *Bone Joint J.* 2014;96-B(12):1623-1630.
22. Morales Martinez A, Caliva F, Flament I, et al. Learning osteoarthritis imaging biomarkers from bone surface spherical encoding. *Magnet Reson Med.* 2020;84(4):2190-2203.
23. Kaneko Y, Nozaki T, Yu H, et al. Normal T2 map profile of the entire femoral cartilage using an angle/layer-dependent approach. *J Magn Reson Imaging.* 2015;42(6):1507-1516.
24. Mosher TJ, Smith H, Dardzinski BJ, Schmithorst VJ, Smith MB. MR imaging and T2 mapping of femoral cartilage: in vivo determination of the magic angle effect. *American Journal of Roentgenology.* 2001;177(3):665-669.
25. Jeffery A, Blunn G, Archer C, Bentley G. Three-dimensional collagen architecture in bovine articular cartilage. *The Journal of bone and joint surgery British volume.* 1991;73(5):795-801.
26. Zheng S, Xia Y, Badar F. Further studies on the anisotropic distribution of collagen in articular cartilage by μMRI. *Magnet Reson Med.* 2011;65(3):656-663.
27. Garnov N, Gründer W, Thörmer G, et al. In vivo MRI analysis of depth - dependent ultrastructure in human knee cartilage at 7 T. *NMR in Biomedicine.* 2013;26(11):1412-1419.
28. Mlynárik V, Degrassi A, Toffanin R, Vittur F, Cova M, Pozzi-Mucelli RS. Investigation of laminar appearance of articular cartilage by means of magnetic resonance microscopy. *Magnetic resonance imaging.* 1996;14(4):435-442.
29. Xia Y. Relaxation anisotropy in cartilage by NMR microscopy (muMRI) at 14-microm resolution. *Magn Reson Med.* 1998;39(6):941-949.
30. Grunder W. MRI assessment of cartilage ultrastructure. *NMR Biomed.* 2006;19(7):855-876.
31. Benninghoff A. Form und Bau der gelenkknorpel in ihren Beziehungen zur funktion-Erste Mitteilung: Die modellierenden und formerhaltenden Faktoren des Knorpelreliefs. *Zeitsh f Anatomie.* 1925;76:43-63.
32. Hennel JW, Klinowski J. Magic-angle spinning: a historical perspective. *New techniques in solid-state NMR*: Springer; 2005:1-14.
33. Geerts-Ossevoort; L, Weerdt; Ed, Duijndam; A, et al. Compressed SENSE. Speed done right. Every time. https://philipsproductcontent.blob.core.windows.net/assets/20180109/619119731f2a42c4acd4a863008a46c7.pdf. 2018;

https://philipsproductcontent.blob.core.windows.net/assets/20180109/619119731f2a42c4acd4a863008a46c7.pdf. Accessed 09/20, 2019.
34. Yushkevich PA, Piven J, Hazlett HC, et al. User-guided 3D active contour segmentation of anatomical structures: significantly improved efficiency and reliability. *Neuroimage.* 2006;31(3):1116-1128.
35. Markwardt CB. "Non-linear least-squares fitting in IDL with MPFIT", in proc. Astronomical Data Analysis Software and Systems XVIII, Quebec, Canada, ASP Conference Series, Vol. 411, eds. D. Bohlender, P. Dowler & D. Durand (Astronomical Society of the Pacific: San Francisco), p. 251-254. 2009.
36. Ahearn TS, Staff RT, Redpath TW, Semple SIK. The use of the Levenberg–Marquardt curve-fitting algorithm in pharmacokinetic modelling of DCE-MRI data. *Physics in Medicine & Biology.* 2005;50(9):N85.
37. Shapiro E, Borthakur A, Kaufman J, Leigh J, Reddy R. Water distribution patterns inside bovine articular cartilage as visualized by1H magnetic resonance imaging. *Osteoarthritis and Cartilage.* 2001;9(6):533-538.
38. Berberat JE, Nissi MJ, Jurvelin JS, Nieminen MT. Assessment of interstitial water content of articular cartilage with T1 relaxation. *Magn Reson Imaging.* 2009;27(5):727-732.
39. Xia Y. MRI of articular cartilage at microscopic resolution. *Bone & joint research.* 2013;2(1):9-17.
40. Xia Y, Moody JB, Alhadlaq H. Orientational dependence of T2 relaxation in articular cartilage: A microscopic MRI (microMRI) study. *Magn Reson Med.* 2002;48(3):460-469.
41. Mlynárik V, Mosher T, Smith H, Dardzinski B. Magic angle effect in articular cartilage. *AJR-American Journal of Roentgenology.* 2002;178(5):1287.
42. Goodwin DW, Dunn JF. MR imaging and T2 mapping of femoral cartilage. *AJR American Journal of Roentgenology.* 2002;178(6):1568-1569; author reply 1569.
43. Nozaki T, Kaneko Y, Hon JY, et al. T1rho mapping of entire femoral cartilage using depth- and angle-dependent analysis. *European radiology.* 2016;26(6):1952-1962.
44. Henkelman RM, Stanisz GJ, Kim JK, Bronskill MJ. Anisotropy of NMR properties of tissues. *Magn Reson Med.* 1994;32(5):592-601.
45. Pang Y. Anisotropic transverse relaxation in the human brain white matter induced by restricted rotational diffusion. In: Proceedings of the 29th Virtual Annual Meeting of ISMRM, 2021. (abstract: 1711).
46. Wang N, Mirando AJ, Cofer G, Qi Y, Hilton MJ, Johnson GA. Characterization complex collagen fiber architecture in knee joint using high‐resolution diffusion imaging. *Magnet Reson Med.* 2020;84(2):908-919.
47. Wei H, Gibbs E, Zhao P, et al. Susceptibility tensor imaging and tractography of collagen fibrils in the articular cartilage. *Magnet Reson Med.* 2017;78(5):1683-1690.
48. Mlynarik V, Szomolanyi P, Toffanin R, Vittur F, Trattnig S. Transverse relaxation mechanisms in articular cartilage. *J Magn Reson.* 2004;169(2):300-307.

SEVEN FIGURE CAPTIONS

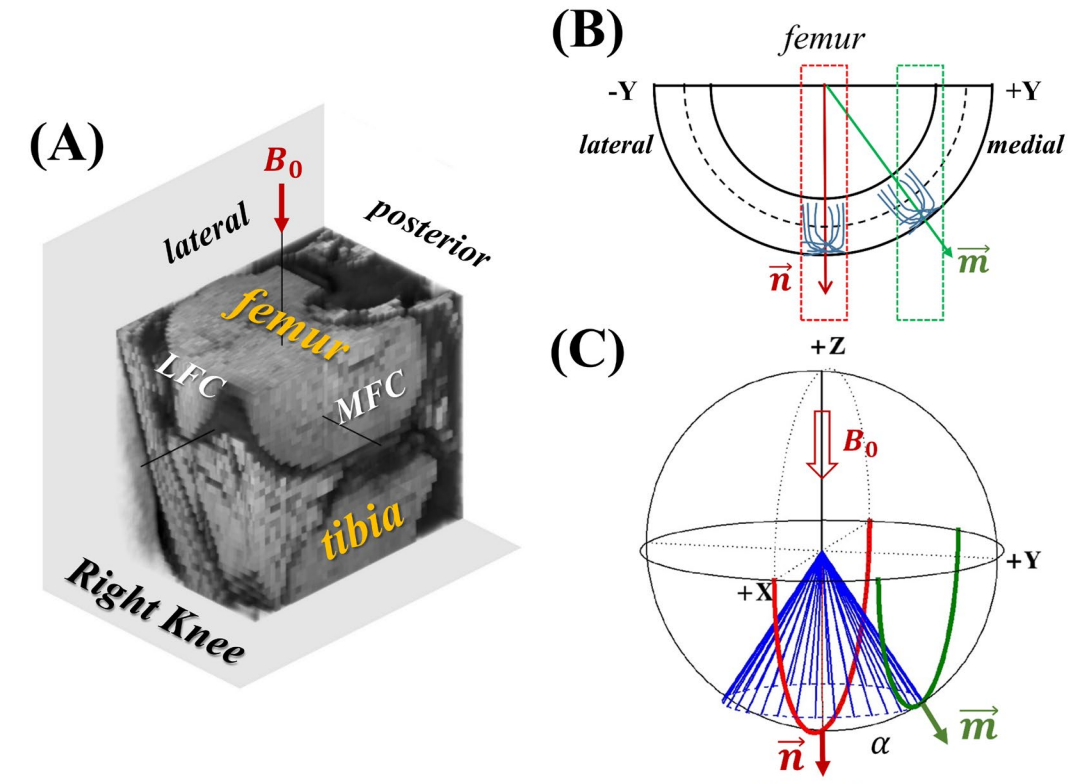

FIGURE 1 A partial volume-rendered high-resolution image of an adult human right knee (A). Two schematic sagittal imaging slices cutting through one femoral condyle's center (red) and off-center (green) in two-dimensional (coronal view) (B) and three-dimensional (unit sphere) diagrams (C) assuming a spherical surface of cartilage. LFC, lateral femoral condyle; MFC, medial femoral condyle

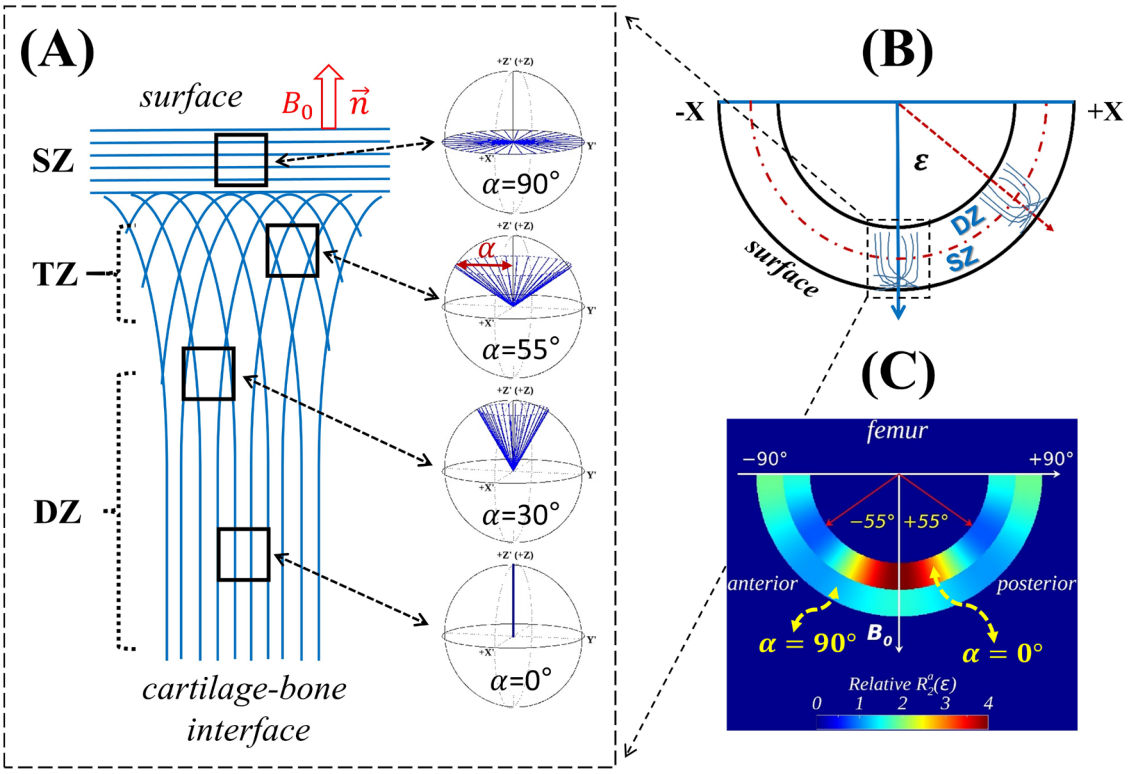

FIGURE 2 Schematics of two-dimensional arcade and three-dimensional funnel models with varying collagen fibril distributions (A) taken from an ideal sagittal imaging slice (B) exhibiting characteristic R_2 orientation-dependences in two segmented cartilage zones (C). DZ, deep zone; SZ, superficial zone; TZ, transitional zone

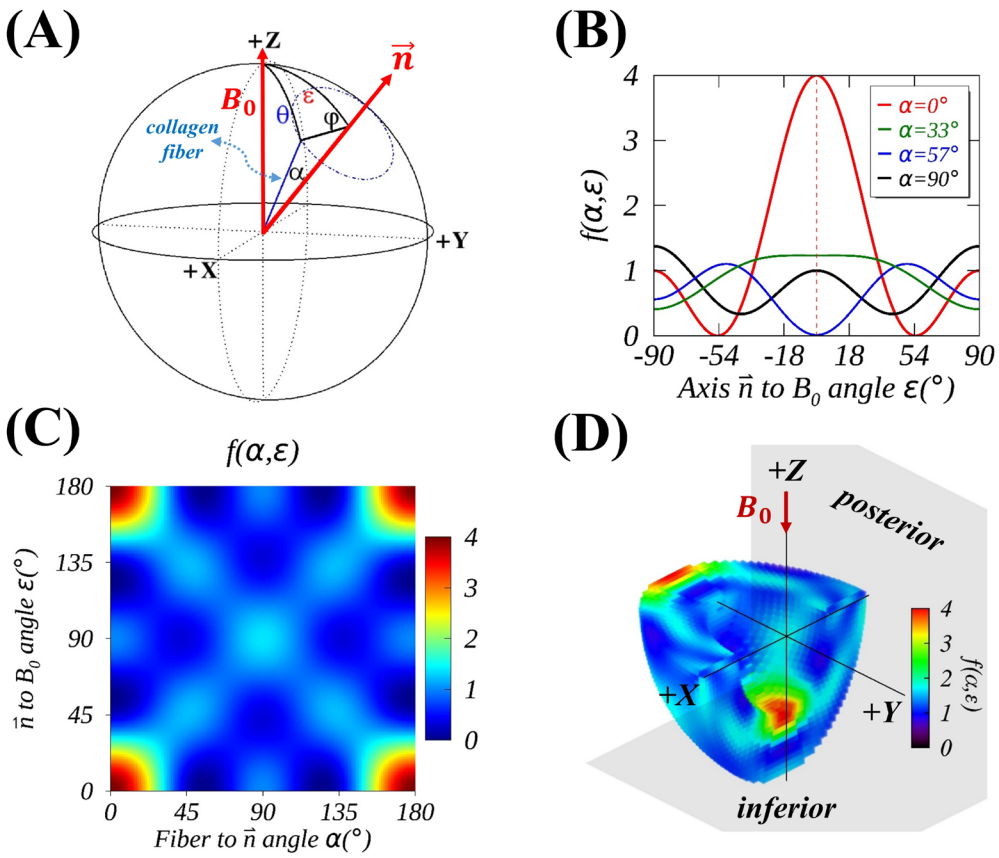

FIGURE 3 An axially symmetric model (A) for collagen fibril distributions with cartilage surface normal denoted by $\vec{n}$. An orientation dependent function $f(\alpha, \varepsilon)$ is depicted by four line profiles (B) with α=0° (red), 33° (green), 57° (blue) and 90° (black), by a 2D map (C) with α=ε =0-180°, and by a multiple (n=11) layers quarter-sphere (D) with α=0-90° from the innermost to outermost layers.

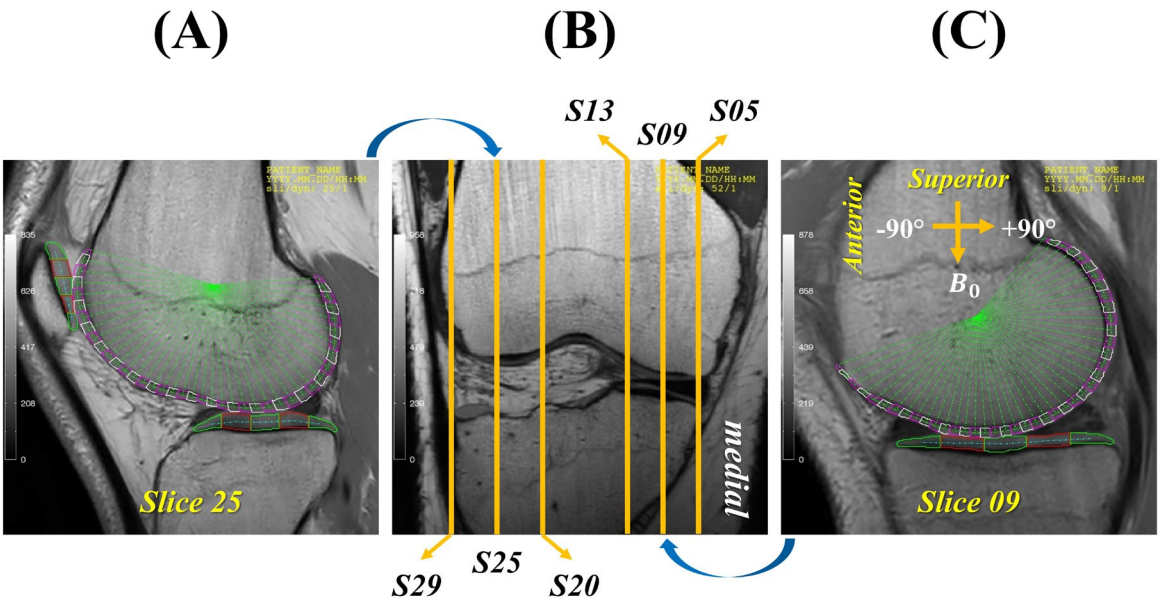

FIGURE 4 A high-resolution coronal image of an adult human right knee (B) with labeled locations for acquired sagittal imaging slices from lateral (Slices 20, 25 and 29) and medial (Slices 05, 09 and 13) femoral condyles. The sagittal images of central Slices 25 (A) and 09 (C) are displayed with angularly and radially segmented ROIs superimposed

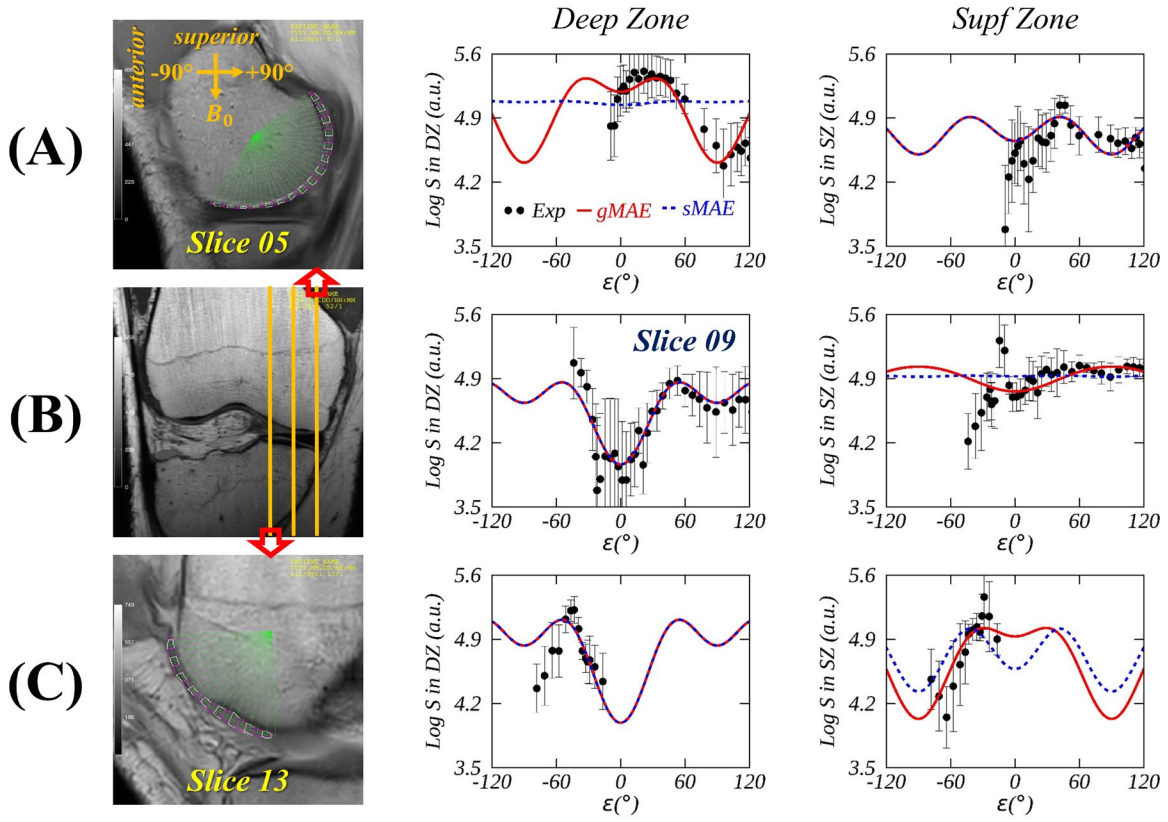

FIGURE 5 Measured (black circles) and fitted (gMAE, solid red lines; sMAE, dashed blue lines) average T2W signal intensities in the deep (2nd column) and superficial zones (3rd column) for Slices 05 (A), 09 (B, Fig. 4C) and 13 (C) from medial knee cartilage (1st column)

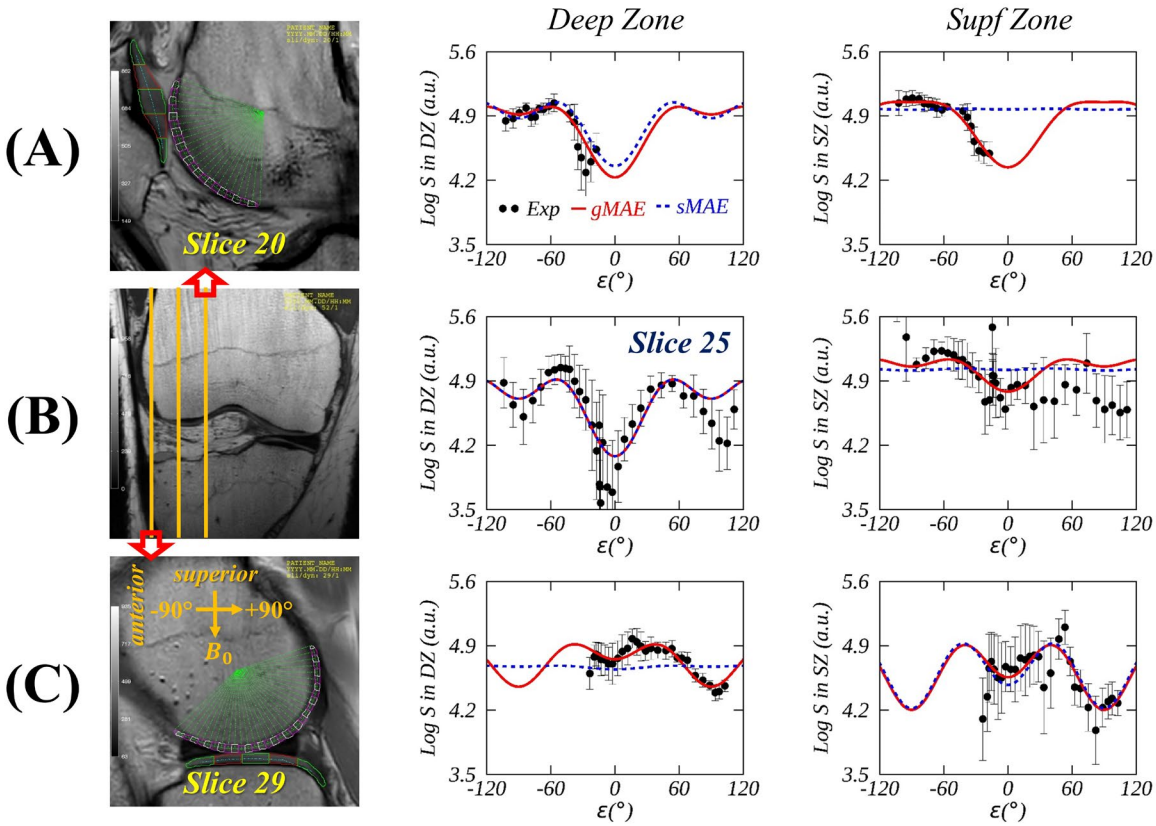

FIGURE 6 Measured (black circles) and fitted (gMAE, solid red lines; sMAE, dashed blue lines) average T2W signal intensities in the deep (2nd column) and superficial zones (3rd column) for Slices 20 (A), 25 (B, Fig. 4A) and 29 (C) from lateral knee cartilage (1st column)

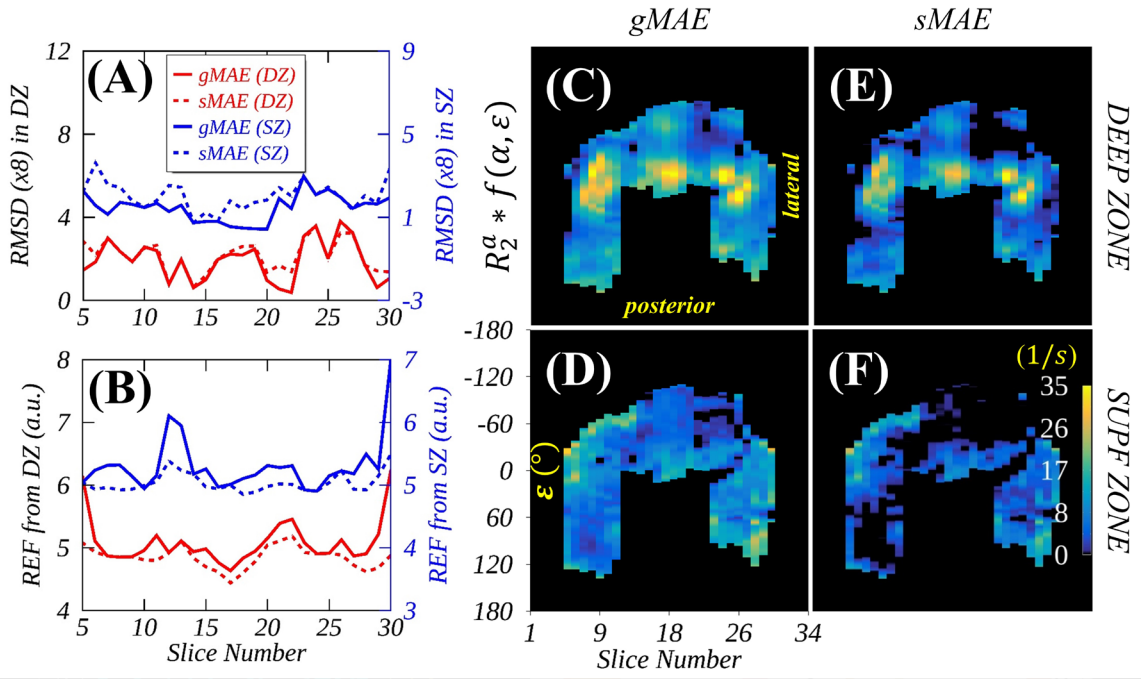

FIGURE 7 Comparisons of the root-mean-square deviations (RMSDs in A) and the fitted model parameter A (REFs in B) for all imaging slices between gMAE (solid lines) and sMAE (dashed lines) in the DZ (red) and SZ (blue). Anisotropic R_2 parametric maps are shown using averaged REFs from gMAE (C and D) and sMAE (E and F) in the DZ (C and E) and SZ (D and F). DZ, deep zone; REF, internal reference; SZ, superficial zone

ONE TABLE

TABLE 1 Fitted model parameters, A (a.u.), B (a.u.) and α (°), from segmented T2W signal profiles in Figures 5 and 6 for the deep (DZ) and superficial (SZ) zones of the femoral cartilage from one adult subject's healthy knee.

Slice index	*Zone*	*gMAE*				*sMAE*			
		A	***B***	***α (°)***	***RMSD***	***A***	***B***	***RMSD***	***P***
5	*DZ*	*6.13±0.20*	*1.52±0.28*	*75±1*	*0.183*	*5.08±0.05*	*0.01±0.00*	*0.356*	*0.001*
	SZ	*5.04±0.15*	*0.39±0.18*	*90±5*	*0.283*	*5.04±0.08*	*0.39±0.10*	*0.283*	*1.000*
9	*DZ*	*4.86±0.07*	*0.22±0.05*	*0±0*	*0.233*	*4.86±0.07*	*0.22±0.05*	*0.233*	*1.000*
	SZ	*5.14±0.08*	*0.24±0.09*	*30±2*	*0.203*	*4.94±0.02*	*0.01±0.00*	*0.225*	*0.760*
13	*DZ*	*5.11±0.07*	*0.28±0.07*	*0±0*	*0.246*	*5.11±0.07*	*0.28±0.07*	*0.246*	*1.000*
	SZ	*5.95±0.32*	*1.74±0.51*	*74±1*	*0.198*	*5.24±0.13*	*0.66±0.26*	*0.305*	*0.148*
20	*DZ*	*5.15±0.06*	*0.36±0.10*	*21±2*	*0.121*	*5.05±0.04*	*0.17±0.05*	*0.170*	*0.297*
	SZ	*5.31±0.06*	*0.50±0.07*	*27±1*	*0.054*	*4.98±0.02*	*0.01±0.00*	*0.229*	*0.000*
25	*DZ*	*4.92±0.04*	*0.21±0.03*	*0±0*	*0.251*	*4.92±0.04*	*0.21±0.03*	*0.251*	*1.000*
	SZ	*5.15±0.08*	*0.10±0.09*	*11±17*	*0.295*	*5.04±0.09*	*0.02±0.10*	*0.307*	*0.916*
29	*DZ*	*5.22±0.07*	*0.64±0.09*	*77±1*	*0.50*	*4.68±0.02*	*0.01±0.00*	*3.90*	*0.000*
	SZ	*5.25±0.18*	*0.82±0.22*	*81±2*	*0.205*	*5.15±0.14*	*0.68±0.15*	*0.209*	*0.820*

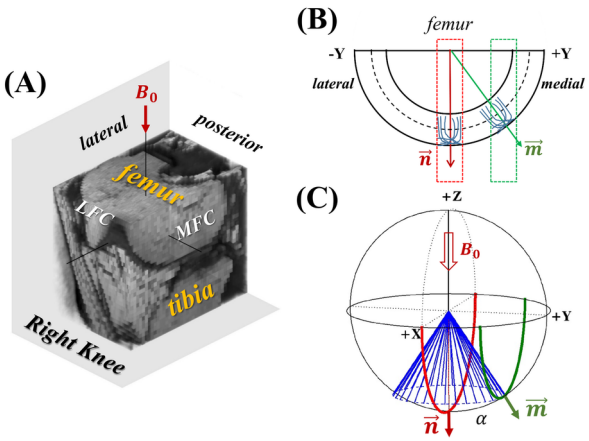

NBM_4535_Slide1.TIF

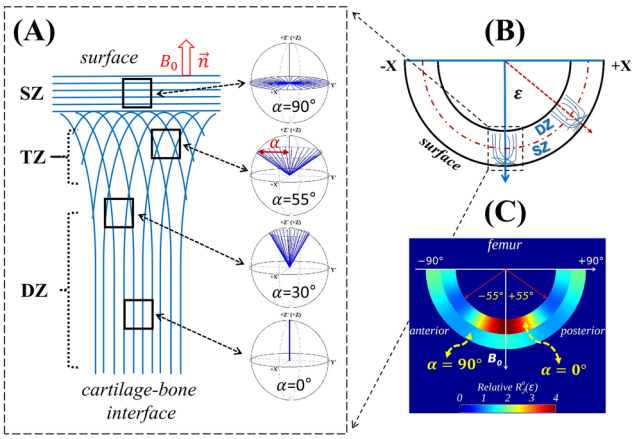

NBM_4535_Slide2.TIF

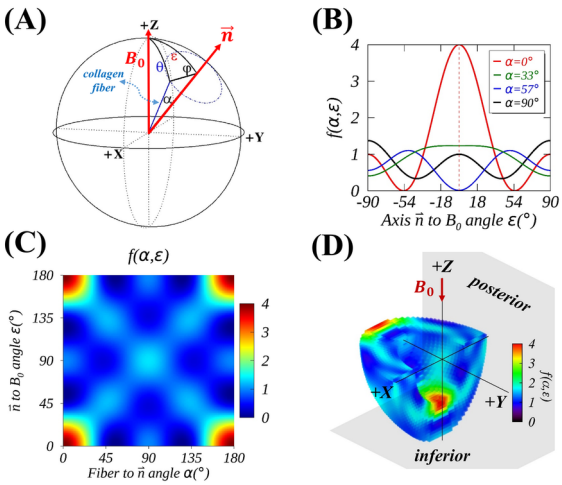

NBM_4535_Slide3.TIF

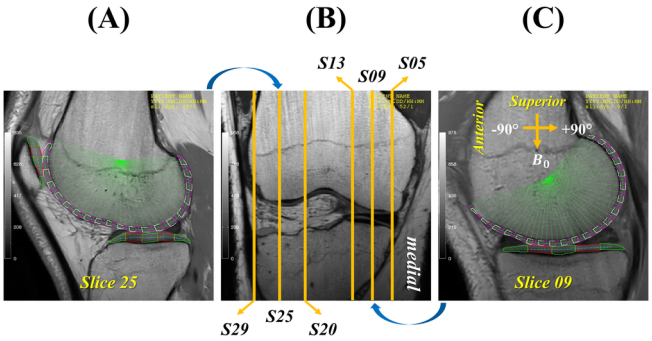

NBM_4535_Slide4.TIF

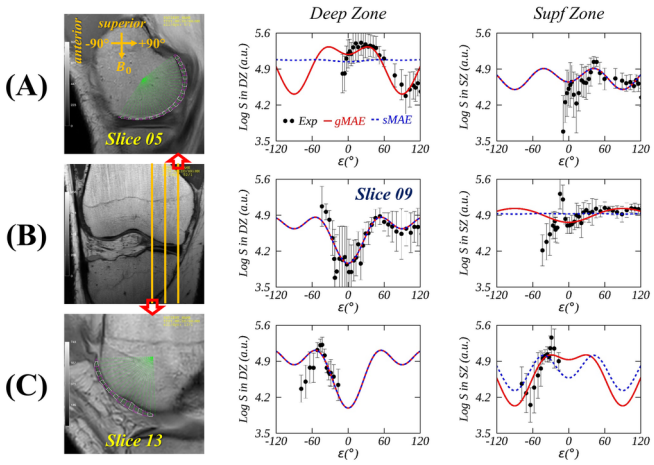

NBM_4535_Slide5.TIF

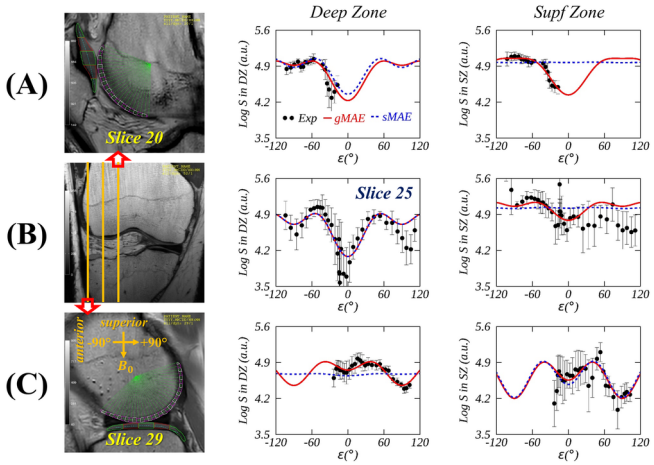

NBM_4535_Slide6.TIF

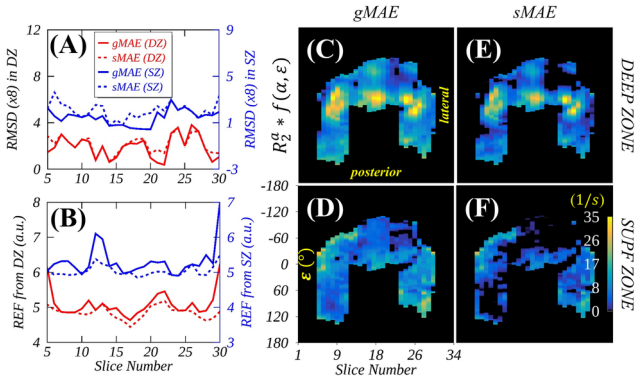

NBM_4535_Slide7.TIF

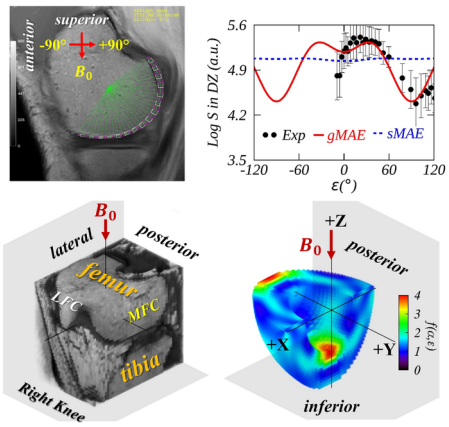

NBM_4535_Slide8.TIF